Preparation, characterization, and catalytic activity of H$_5$PMo$_{10}$V$_2$O$_{40}$ immobilized on nitrogen-containing mesoporous carbon (PMo$_{10}$V$_2$/N-MC) for selective conversion of methanol to dimethoxymethane

Heesoo Kim*, Dong Ryul Park*, Sunyoung Park*, Ji Chul Jung*, Sang-Bong Lee**, and In Kyu Song*,†

*School of Chemical and Biological Engineering, Institute of Chemical Processes, Seoul National University,
Shinlim-dong, Gwanak-gu, Seoul 151-744, Korea
**Korea Research Institute of Chemical Technology, Daejeon 305-600, Korea

Abstract–Nitrogen-containing mesoporous carbon (N-MC) was synthesized by a templating method using SBA-15 and polypyrrole as a templating agent and a carbon precursor, respectively. The N-MC was then modified to have a positive charge, and thus, to provide a site for the immobilization of [PMo$_{10}$V$_2$O$_{40}$]$^{5-}$. By taking advantage of the overall negative charge of [PMo$_{10}$V$_2$O$_{40}$]$^{5-}$, H$_5$PMo$_{10}$V$_2$O$_{40}$ (PMo$_{10}$V$_2$) catalyst was chemically immobilized on the N-MC support as a charge-matching component. Characterization results showed that nitrogen in the N-MC played an important role in forming a nitrogen-derived functional group (amine group), and PMo$_{10}$V$_2$ catalyst was finely and chemically immobilized on the nitrogen-derived functional group of N-MC support. In the vapor-phase selective conversion of methanol, the PMo$_{10}$V$_2$/N-MC catalyst showed a higher conversion of methanol than the bulk PMo$_{10}$V$_2$ catalyst. Furthermore, the PMo$_{10}$V$_2$/N-MC catalyst showed a higher selectivity for dimethoxymethane (a product formed by bifunctional oxidation-acid-acid catalysis) and a higher selectivity for methylformate (a product formed by bifunctional oxidation-acid-oxidation catalysis) than the PMo$_{10}$V$_2$ catalyst. Reaction pathway for selective conversion of methanol to dimethoxymethane over PMo$_{10}$V$_2$/N-MC catalyst could be controlled by changing the methanol feed rate.

Key words: Heteropolyacid, Nitrogen-containing Mesoporous Carbon, Chemical Immobilization, Selective Conversion of Methanol, Dimethoxymethane

INTRODUCTION

Dimethoxymethane (DMM) has attracted much attention in the chemical and energy industries [1] because it is potentially available as a fuel additive due to its high oxygen content and high cetane number [2]. DMM has also been used as a solvent in pharmaceutical and cosmetic industries due to its low toxicity [3]. Furthermore, hydrogen production by reforming of DMM for fuel cell has been recognized as a clean and compact process, because of high hydrogen content and nonpoisonous property of DMM [4]. Easy handling and storage nature of DMM under atmospheric pressure also makes it a good candidate as a hydrogen source for fuel processor [4].

DMM has been synthesized by acetalization of methanol with formaldehyde over acid catalysts [5,6]. Another promising method for obtaining DMM is to convert methanol directly to DMM over bifunctional catalysts with both acid and redox properties. For the direct and selective conversion of methanol to DMM, RuO$_2$ [7], ReO$_x$-based catalyst [8], V$_2$O$_5$/TiO$_2$ [9], and supported heteropolyacid (HPA) catalyst [10] have been investigated. In particular, a supported HPA catalyst [11] and a modified HPA catalyst [12] have been reported to show high DMM selectivity due to their favorable bifunctional acid and redox functions. The selective conversion of methanol to DMM has also been investigated as a model reaction to probe the acid and redox catalytic properties of HPA catalysts [10-12].

HPAs are early transition metal-oxygen anion clusters that have found successful applications in homogeneous and heterogeneous catalysis [13-21]. Among various HPA structural classes, the Keggin HPAs have been widely employed for acid-base and oxidation reactions [13-21]. One of the great advantages of HPAs is that their acid-base and redox properties can be controlled in a systematic way by changing the identity of counter-cation, central heteroatom, and framework polyatom [22-27]. A disadvantage of HPA catalysts, however, is that their surface area is too low (<10 m^2/g). To overcome the low surface area, HPA catalysts have been conventionally supported on various inorganic materials such as silica [28], titania [29], and carbon [30]. Another promising approach for increasing surface area of HPA catalysts is to take advantage of the overall negative charge of heteropolyanions. By this method, HPAs have been successfully immobilized on polymer materials such as poly-4-vinylpyridine, polyaniline, and polystyrene [31-33]. HPAs have also been chemically immobilized on aminopropyl-functionalized mesoporous silica [34,35] and mesostructured cellular foam silica through a grafting method [36].

Highly ordered mesoporous carbon materials have high surface area, large pore volume, and uniform pore size distribution [37-39]. Although it is difficult to form a positive charge on mesoporous carbon materials due to their hydrophobic nature and chemical inertness, mesoporous carbon materials still have a merit as a catalyst support due to their high conductivity, excellent thermal stability, and controllable textural properties [37-39]. If mesoporous carbon materials are easily modified to have a positive charge, they can serve

as efficient supports for HPA catalysts.

In this work, nitrogen-containing mesoporous carbon (N-MC) was synthesized by a templating method using SBA-15 and poly-pyrrole as a templating agent and a carbon precursor, respectively. The N-MC was then modified to have a positive charge for the immobilization of [PMo$_{10}$V$_2$O$_{40}$]$^{5-}$. By taking advantage of the overall negative charge of [PMo$_{10}$V$_2$O$_{40}$]$^{5-}$, H$_5$PMo$_{10}$V$_2$O$_{40}$ (PMo$_{10}$V$_2$) HPA catalyst was chemically immobilized on the N-MC support as a charge-matching component. The PMo$_{10}$V$_2$/N-MC catalyst was characterized and applied to the selective conversion of methanol to DMM.

EXPERIMENTAL

1. Preparation of Nitrogen-containing Mesoporous Carbon (N-MC)

Highly ordered mesoporous SBA-15 was synthesized for use as a templating material for nitrogen-containing mesoporous carbon (N-MC) according to the method reported in the literature [40]. N-MC was then synthesized as follows. FeCl$_3$ (1.0 g) dissolved in an aqueous HCl solution (1.5 ml, 1.0 M) was impregnated on SBA-15 (1.0 g) by an incipient wetness method. The resulting yellow-colored slurry was dried at 100 °C in a convection oven to obtain a solid. The solid was reacted with pyrrole monomer (0.5 g) at room temperature under vacuum condition for the polymerization of pyrrole. The composite of SBA-15 and polypyrrole was dried at 80 °C, and then it was carbonized at 900 °C for 5 h in a stream of nitrogen (40 ml/min). Silica template and FeCl$_3$ were removed by the treatment with HF and HNO$_3$. After the resulting solid was washed with deionized water several times, the solid was finally dried at 100 °C in a convection oven to yield the N-MC.

2. Immobilization of H$_5$PMo$_{10}$V$_2$O$_{40}$ (PMo$_{10}$V$_2$) Catalyst on Nitrogen-containing Mesoporous Carbon (N-MC)

Fig. 1 shows the schematic procedures for the surface modification of N-MC and the subsequent immobilization of PMo$_{10}$V$_2$ on the N-MC. N-MC (1.0 g) was activated by flowing hydrogen (10 ml/min) at 200 °C for 2 h to create amine groups on the surface of

N-MC. The activated N-MC was then treated with an aqueous HCl solution (pH<4) for 12 h to form a positive charge. After washing the resulting N-MC with deionized water several times, it was dried overnight at 100 °C to yield the surface-modified N-MC. For the preparation of PMo$_{10}$V$_2$ catalyst immobilized on N-MC (PMo$_{10}$V$_2$/N-MC), PMo$_{10}$V$_2$ (1.0 g) and surface-modified N-MC (1.0 g) were dissolved in acetonitrile (100 ml). The pH of the mixed slurry was maintained below 2.0 by using an aqueous HCl solution. The slurry was stirred for 24 h at room temperature for the immobilization of PMo$_{10}$V$_2$ on the surface-modified N-MC. After the solid product was recovered by filtration, it was washed with deionized water several times until the washing solvent became colorless. The solid product was dried at 100 °C overnight, and then it was calcined at 200 °C for 3 h to yield the PMo$_{10}$V$_2$/N-MC.

3. Characterization

The nature of the functional group on the N-MC was confirmed by X-ray photoelectron spectroscopy (XPS) measurements (KRATTOS, AXIS). Acid properties of unsupported PMo$_{10}$V$_2$ and PMo$_{10}$V$_2$/N-MC catalysts were determined by NH$_3$-TPD experiments. For the TPD measurements, each catalyst (either unsupported PMo$_{10}$V$_2$ or PMo$_{10}$V$_2$/N-MC, 30 mg on PMo$_{10}$V$_2$ basis) was charged into a quartz reactor of a conventional TPD apparatus. The sample was pretreated at 200 °C for 2 h under flow helium (20 ml/min) in order to remove any physisorbed molecules. NH$_3$ (20 ml) was then pulsed into the reactor every minute at room temperature under a flow of helium (5 ml/min), until the acid sites of the catalyst were saturated with NH$_3$. The physisorbed NH$_3$ was removed by evacuating the catalyst sample at 100 °C for 1 h. The sample was heated from room temperature to 400 °C at a rate of 5 °C/min under a flow of helium (10 ml/min). The desorbed NH$_3$ was detected by using a GC-MSD (Agilent, 5975 MSD-6890N GC).

4. Vapor-phase Selective Conversion of Methanol to Dimethoxymethane

Vapor-phase selective conversion of methanol to dimethoxymethane (DMM) was performed in a continuous flow fixed-bed reactor at atmospheric pressure. 1.2 g of unsupported PMo$_{10}$V$_2$ or 1.2 g of
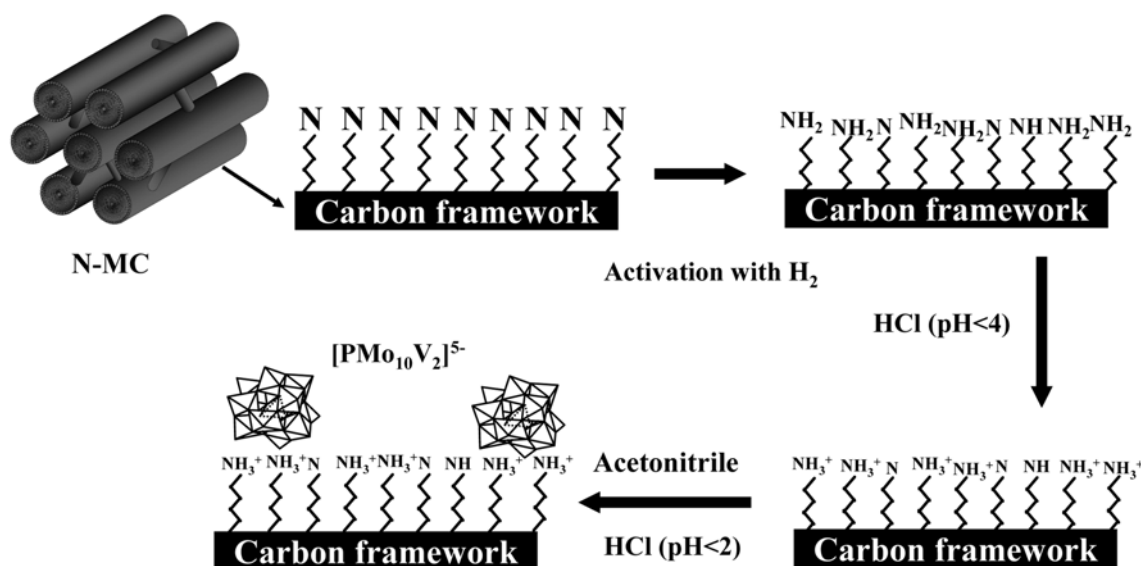

Fig. 1. Schematic procedures for the surface modification of N-MC and the subsequent immobilization of PMo$_{10}$V$_2$ on the N-MC.

PMo$_{10}$V$_2$/N-MC (net amount of PMo$_{10}$V$_2$=0.158 g) was charged into a tubular quartz reactor, and then it was pretreated with a nitrogen (20 ml/min) at 240 °C for 1 h. Methanol (1.0 ml/h) was sufficiently vaporized by passing through a pre-heating zone and was continuously fed into the reactor together with a mixed stream of oxygen (5 ml/min) and nitrogen carrier (20 ml/min). Contact times were maintained at 6.4 and 48.6 g-PMo$_{10}$V$_2$-h/methanol-mole for PMo$_{10}$V$_2$/N-MC and PMo$_{10}$V$_2$ catalysts, respectively. The catalytic reaction was carried out at 220 °C for 5 h. The catalytic performance of PMo$_{10}$V$_2$/N-MC was further examined by changing the methanol feed rate from 0.3 to 1.0 ml/h. The reaction products were periodically sampled and analyzed with an on-line gas chromatograph (HP 5890 II). Conversion of methanol and selectivity for products were calculated on the basis of mole balance.

RESULTS AND DISCUSSION

1. Characterization of N-MC Support and PMo$_{10}$V$_2$/N-MC Catalyst

Fundamental characterization results for N-MC support and PMo$_{10}$V$_2$/N-MC catalyst were reported in our previous work [41]. Surface area, pore volume, and average pore diameter of N-MC were found to be 940 m^2/g, 1.0 cm^3/g, and 3.8 nm, respectively. PMo$_{10}$V$_2$/N-MC still retained relatively high surface area (=727 m^2/g), large pore volume (=0.78 cm^3/g), and uniform pore size distribution (=3.8 nm) even after the immobilization of PMo$_{10}$V$_2$. The loading of PMo$_{10}$V$_2$ in the PMo$_{10}$V$_2$/N-MC was 13.2 wt%.

Chemical immobilization of PMo$_{10}$V$_2$ on the N-MC support was confirmed by FT-IR analyses. It was observed that the characteristic IR bands of PMo$_{10}$V$_2$ in the PMo$_{10}$V$_2$/N-MC appeared at slightly shifted positions compared to those of unsupported PMo$_{10}$V$_2$ [41]. This result indicates that PMo$_{10}$V$_2$ was successfully immobilized on the N-MC via strong chemical interaction between the two components.

Two distinct bands of N-MC support were found at around 1,350 cm^{-1} (D-band) and 1,580 cm^{-1} (G-band) in the Raman spectrum. The peak area of the G-band (characteristic band of graphitic structure) was much larger than that of the D-band (characteristic band of disorder-induced scattering) [41]. This indicates that the N-MC support with a graphitic structure was successfully prepared.

Fine dispersion of PMo$_{10}$V$_2$ on the N-MC support was confirmed by XRD analyses. PMo$_{10}$V$_2$/N-MC exhibited no characteristic XRD patterns of PMo$_{10}$V$_2$, but showed almost the same XRD patterns as N-MC, even though 13.2 wt% of PMo$_{10}$V$_2$ was loaded in the PMo$_{10}$V$_2$/N-MC [41]. This result means that PMo$_{10}$V$_2$ species were not in a crystal state but in an amorphous-like state, suggesting that PMo$_{10}$V$_2$ species were finely dispersed on the N-MC.

2. Role of Nitrogen on N-MC Support

Fig. 2(a) shows the XPS spectrum of N-MC support. Three characteristic peaks were observed in the N-MC support at around 284.5 eV (C 1s), 401.2 eV (N 1s), and 532.1 eV (O 1s). The existence of the N 1s peak was attributed to nitrogen in pyrrole (the nitrogen-containing carbon precursor). Fig. 2(b) shows the deconvoluted XPS spectrum for N 1s in the N-MC support. The N 1s peak could be deconvoluted into three characteristic bands appearing at around 398.7±0.2 eV (pyridinic nitrogen), 401.2±0.2 eV (quaternary nitrogen), and 402.9±0.2 eV (nitrogen oxide) [42-44]. Compositions of ni-
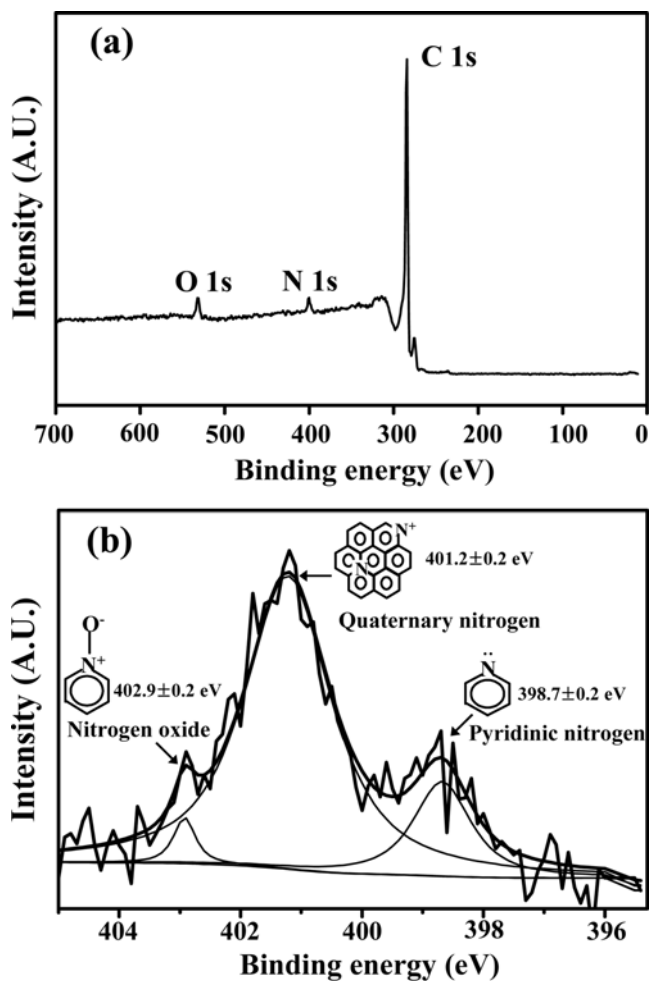
Fig. 2. (a) XPS spectrum of N-MC support and (b) deconvoluted XPS spectrum for N 1s in the N-MC support.

trogen-containing functional groups were found to be 17.0% (pyridinic nitrogen), 79.8% (quaternary nitrogen), and 3.2% (nitrogen oxide), respectively. The formation of nitrogen oxide species was due to the exposure of N-MC to ambient condition after transition from pyrrolic nitrogen species to pyridinic nitrogen and quaternary nitrogen species during the carbonization process. The pyridinic nitrogen exists on the edge of graphitic carbon planes, where it is bonded to two carbon atoms by donating one p electron to the aromatic π-system. The quaternary nitrogen represents nitrogen that is confined in a graphitic plane and bonded to three carbon atoms. The binding energy of quaternary nitrogen was higher than that of pyridinic nitrogen. Furthermore, the composition of quaternary nitrogen was much larger than that of pyridinic nitrogen. These results imply that the edge nitrogen of quaternary nitrogen species can be more favorably and dominantly converted into positively charged nitrogen-containing functional group than nitrogen of pyridinic nitrogen species [42-44]. Thus, it can be inferred that edge nitrogen of quaternary nitrogen species in the N-MC may play an important role in forming a nitrogen-derived functional group (amine group) for the immobilization of PMo$_{10}$V$_2$ catalyst.
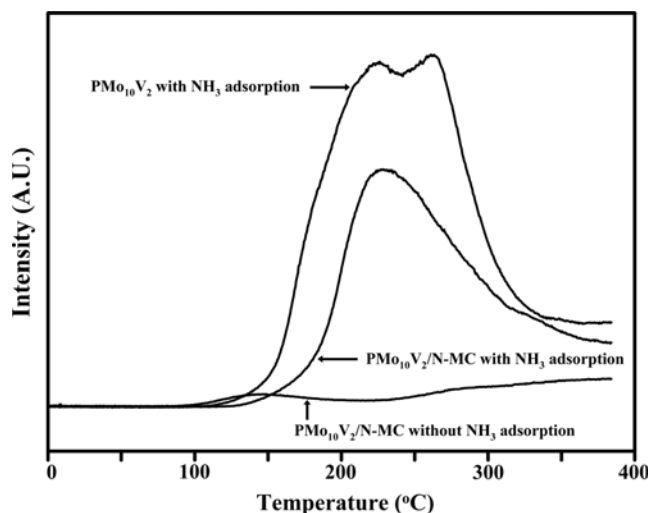
3. Acid Properties of Unsupported PMo$_{10}$V$_2$ and PMo$_{10}$V$_2$/N-MC

Fig. 3. NH₃-TPD profiles of unsupported $PMo_{10}V_2$ and $PMo_{10}V_2/$ N-MC catalysts.

Fig. 5. Catalytic performance of unsupported $PMo_{10}V_2$ (1.2 g on $PMo_{10}V_2$ basis) and $PMo_{10}V_2$/N-MC (0.158 g on $PMo_{10}V_2$ basis) in the vapor-phase selective conversion of methanol to DMM at 220 °C after a 5 h-reaction.

Fig. 3 shows the NH₃-TPD profiles of unsupported $PMo_{10}V_2$ and $PMo_{10}V_2$/N-MC catalysts. The maximum desorption peak temperature of both catalysts was observed at around 220 °C. This indicates that acid strength of $PMo_{10}V_2$/N-MC was almost identical to that of unsupported $PMo_{10}V_2$. The peak area of unsupported $PMo_{10}V_2$ was much larger than that of $PMo_{10}V_2$/N-MC. This result means that acid amount of $PMo_{10}V_2$ catalyst was reduced via chemical immobilization on the N-MC support. To ensure the immobilized state of $PMo_{10}V_2$ on the N-MC more accurately, additional NH₃-TPD measurement for $PMo_{10}V_2$/N-MC in the absence of NH₃ adsorption was conducted. As shown in Fig. 3, the $PMo_{10}V_2$/N-MC catalyst in the absence of NH₃ adsorption showed a small and broad desorption peak due to the decomposition of nitrogen-derived functional group (-NH₃⁺). The peak area of NH₃-TPD profile observed for $PMo_{10}V_2$/N-MC with NH₃ adsorption corresponds to the amount of NH₃ originating from the decomposition of amine functional group and the chemically adsorbed NH₃ on the acid sites of $PMo_{10}V_2$/N-MC. Therefore, the difference in NH₃-TPD peak area between $PMo_{10}V_2$/N-MC with NH₃ adsorption and $PMo_{10}V_2$/N-MC without NH₃ adsorption is equivalent to the pure acid sites existing in the $PMo_{10}V_2$/N-MC. The peak area of NH₃-TPD profile observed for unsupported $PMo_{10}V_2$ corresponds to the amount of NH₃ adsorbed on the acid sites of $PMo_{10}V_2$. The amount of adsorbed NH₃ obtained by sub-
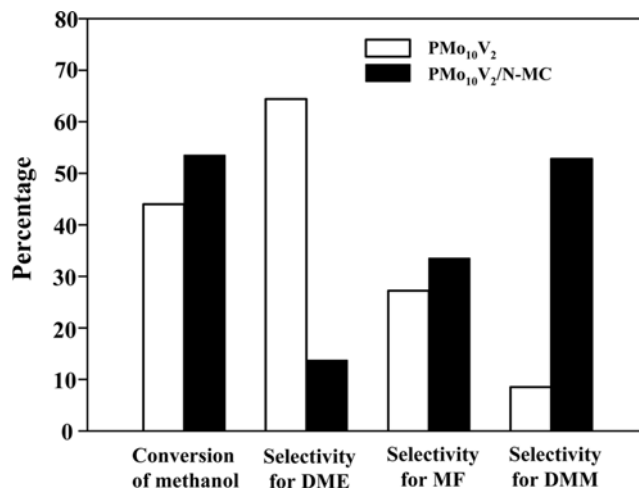
tracting the peak area of $PMo_{10}V_2$/N-MC in the absence of NH₃ adsorption from the peak area of $PMo_{10}V_2$/N-MC with NH₃ adsorption was found to be 48% of the amount of NH₃ adsorbed on the unsupported $PMo_{10}V_2$ catalyst. A simple calculation based on the pure acid amounts of $PMo_{10}V_2$/N-MC and unsupported $PMo_{10}V_2$ revealed that the actual chemical state of $PMo_{10}V_2$ immobilized on the N-MC was $H_{2.4}(\sim NH_3)_{2.6}PMo_{10}V_2O_{40}$/N-MC. This result means that $PMo_{10}V_2$ was chemically immobilized on the N-MC support as a charge-matching component by partially losing its protons (acid sites). It should also be noted that the $PMo_{10}V_2$/N-MC catalyst still retains considerable amount of acid sites.

4. Catalytic Performance of $PMo_{10}V_2$/N-MC in the Selective Conversion of Methanol to Dimethoxymethane

Fig. 4 shows the reaction pathway for selective conversion of methanol to DMM over bifunctional oxidation and acid catalyst. It is known that formaldehyde (FA) is produced by oxidation catalysis of HPA, while dimethyl ether (DME) is produced by acid catalysis of HPA in the primary reaction of methanol [10-12]. In the secondary reaction, dimethoxymethane (DMM) is produced via acid-catalyzed reaction of methoxymethanol (MM) intermediate with methanol. As a consequence, DMM is formed from methanol via consecutive bifunctional oxidation-acid-acid catalysis, while MF is
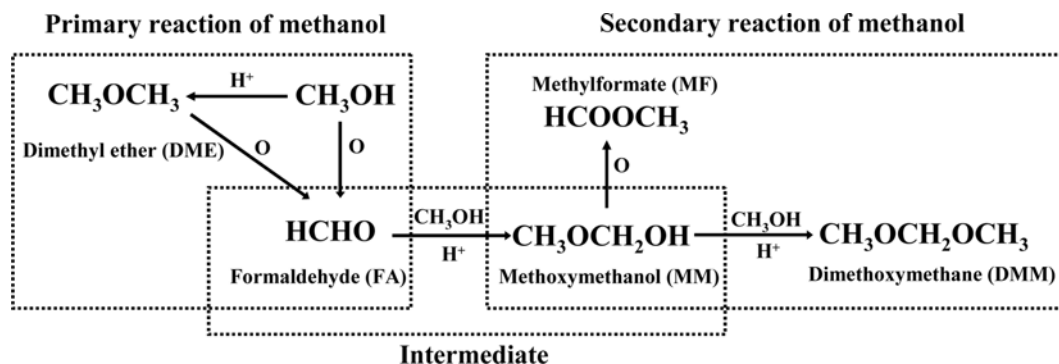

Fig. 4. Reaction pathway for selective conversion of methanol to DMM over bifunctional oxidation and acid catalyst.

produced via consecutive bifunctional oxidation-acid-oxidation catalysis [10-12]. This implies that both well-controlled oxidation and acid catalytic functions are required for the selective conversion of methanol to DMM.

Fig. 5 shows the catalytic performance of unsupported $PMo_{10}V_2$ and $PMo_{10}V_2$/N-MC in the vapor-phase selective conversion of methanol to DMM at 220 °C after a 5 h-reaction. In the catalytic reaction, only a small amount of FA was detected (<2 mole%) and MM was not in a detectable range. This means that FA and MM acted as intermediates in the selective conversion of methanol to DMM (Fig. 4). Furthermore, formation of CO and CO_2 was negligible. Although large amount of bulk $PMo_{10}V_2$ (1.2 g on $PMo_{10}V_2$ basis) was used, the $PMo_{10}V_2$/N-MC (0.158 g on $PMo_{10}V_2$ basis) catalyst showed a higher conversion of methanol than the unsupported $PMo_{10}V_2$ catalyst. The enhanced catalytic performance of $PMo_{10}V_2$/N-MC was due to the fine dispersion of $PMo_{10}V_2$ on the surface of N-MC formed via chemical immobilization. The $PMo_{10}V_2$/N-MC catalyst showed a suppressed selectivity for DME (a product formed by acid catalysis) compared to the mother catalyst. This is because $PMo_{10}V_2$ in the $PMo_{10}V_2$/N-MC was chemically immobilized on the positive site ($-NH_3^+$) of N-MC by partially sacrificing its protons. It is interesting to note from Fig. 5 that the $PMo_{10}V_2$/N-MC catalyst shows a higher selectivity for DMM (a product formed by bifunctional oxidation-acid-acid catalysis) and a higher selectivity for MF (a product formed by bifunctional oxidation-acid-oxidation catalysis) than the $PMo_{10}V_2$ catalyst. This may be due to both enhanced oxidation property (caused by fine dispersion of $PMo_{10}V_2$ species) and moderate acid property of $PMo_{10}V_2$/N-MC catalyst for this complicated reaction requiring both adequate oxidation and acid catalysis. However, the increment of DMM selectivity over $PMo_{10}V_2$/N-MC with respect to $PMo_{10}V_2$ was much larger than the increment of MF selectivity over $PMo_{10}V_2$/N-MC with respect to $PMo_{10}V_2$. In other words, the $PMo_{10}V_2$/N-MC catalyst was much more efficient than the bulk $PMo_{10}V_2$ catalyst in the selective conversion of methanol to DMM.

Fig. 6 shows the catalytic performance of $PMo_{10}V_2$/N-MC in the vapor-phase selective conversion of methanol to DMM at 220 °C with a variation of methanol feed rate. As shown in Fig. 6(a), conversion of methanol slightly decreased with increasing methanol feed rate. This was attributed to the decrease of contact time between catalyst and methanol feed. However, methanol consumption rate linearly increased with increasing methanol feed rate. This was due to the nature of the secondary reaction that led to the formation of MF and DMM by bimolecular coupling reaction of FA and MM intermediates [7]. Fig. 6(b) shows the selectivities for MF and DMM over $PMo_{10}V_2$/N-MC catalyst with respect to methanol feed rate. DME selectivity over $PMo_{10}V_2$/N-MC catalyst was almost constant, although this was not shown here. It was observed that selectivity for DMM increased and selectivity for MF decreased with increasing methanol feed rate. The enhanced selectivity for DMM at high methanol feed rate was attributed to the accelerated dehydration reaction of MM intermediate with methanol on the acid sites of $PMo_{10}V_2$/N-MC catalyst. On the other hand, MM intermediate was favorably converted into MF at low methanol feed rate through oxidative dehydrogenation reaction on the redox sites of $PMo_{10}V_2$/N-MC catalyst. The above results imply that the reaction pathway for selective conversion of methanol to DMM over $PMo_{10}V_2$/N-MC catalyst can be controlled by changing the methanol feed rate.

CONCLUSIONS

N-MC was synthesized by a templating method using SBA-15 and polypyrrole as a templating agent and a carbon precursor, respectively. The N-MC was then modified to have a positive charge for the immobilization of $[PMo_{10}V_2O_{40}]^{5-}$. By taking advantage of the overall negative charge of $[PMo_{10}V_2O_{40}]^{5-}$, $PMo_{10}V_2$ catalyst was immobilized on the N-MC support as a charge-matching component. Characterization results showed that edge nitrogen of quaternary nitrogen species in the N-MC played an important role in form-
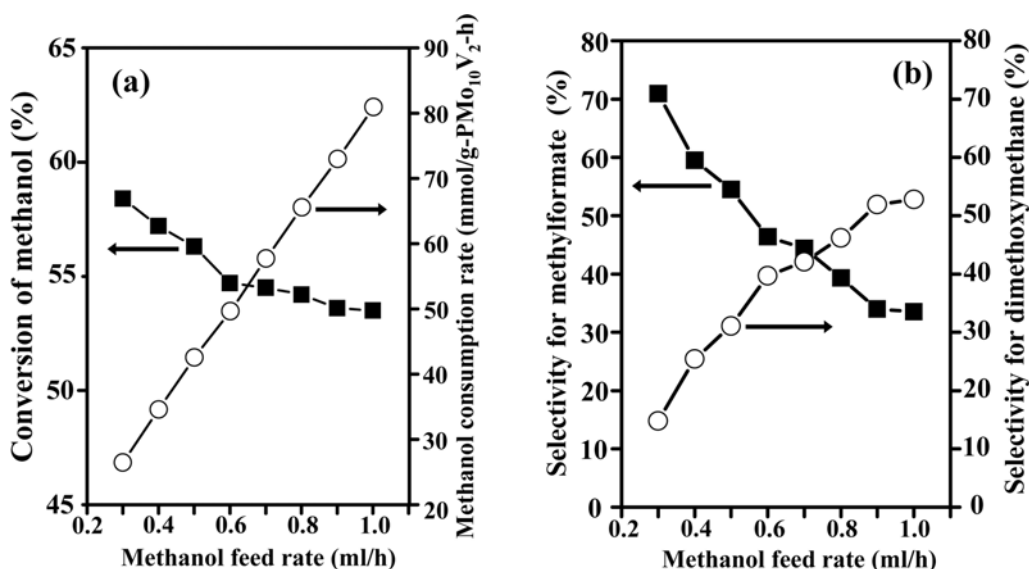

Fig. 6. Catalytic performance of $PMo_{10}V_2$/N-MC (0.158 g on $PMo_{10}V_2$ basis) in the vapor-phase selective conversion of methanol to DMM at 220 °C with a variation of methanol feed rate: (a) conversion of methanol and methanol consumption rate, (b) selectivity for MF and DMM.

ing a nitrogen-derived functional group (amine group) for the immobilization of PMo$_{10}$V$_2$. PMo$_{10}$V$_2$ species were finely and chemically immobilized on the N-MC support by partially sacrificing its protons. Actual chemical state of PMo$_{10}$V$_2$ immobilized on the N-MC was found to be H$_{2.4}$(~NH$_3$)$_{2.6}$PMo$_{10}$V$_2$O$_{40}$/N-MC. In the vapor-phase selective conversion of methanol, the PMo$_{10}$V$_2$/N-MC catalyst showed a higher conversion of methanol and a lower selectivity for DME (a product formed by acid catalysis) than the bulk PMo$_{10}$V$_2$ catalyst. In addition, the PMo$_{10}$V$_2$/N-MC catalyst showed a higher selectivity for DMM (a product formed by bifunctional oxidation-acid-acid catalysis) and a higher selectivity for MF (a product formed by bifunctional oxidation-acid-oxidation catalysis) than the PMo$_{10}$V$_2$ catalyst. This was due to both enhanced oxidation property (caused by fine dispersion of PMo$_{10}$V$_2$ species) and moderate acid property of PMo$_{10}$V$_2$/N-MC catalyst for this complicated reaction requiring both adequate oxidation and acid catalysis. The PMo$_{10}$V$_2$/N-MC catalyst was much more efficient than the bulk PMo$_{10}$V$_2$ catalyst in the selective conversion of methanol to DMM. Selectivity for DMM increased and selectivity for MF decreased with increasing methanol feed rate. Thus, the reaction pathway for selective conversion of methanol to DMM over PMo$_{10}$V$_2$/N-MC catalyst could be controlled by changing the methanol feed rate.

ACKNOWLEDGMENTS

REFERENCES

1. H. S. Liu, C. J. Song, L. Zhang, J. J. Zhang, H. J. Wang and D. P. Wilkinson, *J. Power Sources*, **155**, 95 (2006).
2. G. Renard, P. J. van Tiggelen and J. Vandooren, *Proc. Combust. Inst.*, **29**, 1277 (2002).
3. P. I. Arvidsson, Ö. Davidsson and G. Hilmersson, *Tetrahedron Asymmetry*, **10**, 527 (1999).
4. Y. Fu and J. Shen, *J. Catal.*, **248**, 101 (2007).
5. G. P. Hagen and M. J. Spangler, US Patent 6,265,528 (2001).
6. S. Satoh and Y. Tanigawa, US Patent 6,349,507 (2002).
7. H. Liu and E. Iglesia, *J. Phy. Chem. B*, **109**, 2155 (2005).
8. Y. Yuan, H. Liu, H. Imoto, T. Shido and Y. Iwasawa, *J. Catal.*, **195**, 51 (2000).
9. Y. Fu and J. Shen, *Chem. Commun.*, 2172 (2007).
10. H. Liu and E. Iglesia, *J. Phy. Chem. B*, **107**, 10840 (2003).
11. H. Liu and E. Iglesia, *J. Catal.*, **223**, 161 (2004).
12. H. Liu, N. Bayat and E. Iglesia, *Angew. Chem. Int. Ed.*, **42**, 5072 (2003).
13. I. K. Song, S. H. Moon and W. Y. Lee, *Korean J. Chem. Eng.*, **8**, 33 (1991).
14. S. H. Lee, D. R. Park, H. Kim, J. Lee, J. C. Jung, S. Y. Woo, W. S. Song, M. S. Kwon and I. K. Song, *Korean J. Chem. Eng.*, **25**, 1018 (2008).
15. M. Misono, *Korean J. Chem. Eng.*, **14**, 427 (1997).
16. W. Y. Lee, I. K. Song, J. K. Lee, G. I. Park and S. S. Lim, *Korean J. Chem. Eng.*, **14**, 432 (1997).
17. J. S. Choi, I. K. Song and W. Y. Lee, *Korean J. Chem. Eng.*, **17**, 280 (2000).
18. K. W. La, H. Kim, J. C. Jung, J. Lee, D. R. Park, S. H. Lee and I. K. Song, *Korean J. Chem. Eng.*, **25**, 710 (2008).
19. J. K. Lee, I. K. Song and W. Y. Lee, *Korean J. Chem. Eng.*, **12**, 384 (1995).
20. M. H. Youn, D. R. Park, J. C. Jung, H. Kim, M. A. Barteau and I. K. Song, *Korean J. Chem. Eng.*, **24**, 51 (2007).
21. H. Kim, J. C. Jung, D. R. Park, J. Lee, K. M. Cho, S. Park, S. H. Lee and I. K. Song, *Korean J. Chem. Eng.*, **25**, 231 (2008).
22. I. K. Song and M. A. Barteau, *Korean J. Chem. Eng.*, **19**, 567 (2002).
23. I. K. Song, H. S. Kim and M.-S. Chun, *Korean J. Chem. Eng.*, **20**, 844 (2003).
24. T. Okuhara, N. Mizuno and M. Misono, *Adv. Catal.*, **41**, 113 (1996).
25. C. L. Hill and C. M. Prosser-McCartha, *Coord. Chem. Rev.*, **143**, 407 (1995).
26. I. V. Kozhevnikov, *Chem. Rev.*, **98**, 171 (1998).
27. N. Mizuno and M. Misono, *Chem. Rev.*, **98**, 199 (1998).
28. N.-Y. He, C.-S. Woo, H.-G. Kim and H.-I. Lee, *Appl. Catal. A*, **281**, 167 (2005).
29. J. Poźniczek, A. Lubańska, A. Micek-Ilnicka, D. Mucha, E. Lalik and A. Bilański, *Appl. Catal. A*, **298**, 217 (2006).
30. F. X. Liu-Cai, B. Sahut, E. Faydi, A. Auroux and G. Herve, *Appl. Catal. A*, **185**, 75 (1999).
31. K. Nomiya, H. Murasaki and M. Miwa, *Polyhedron*, **5**, 1031 (1986).
32. M. Hasik, W. Turek, E. Stochmal, M. Łapkowski and A. Proń, *J. Catal.*, **147**, 544 (1994).
33. H. Kim, J. C. Jung, S. H. Yeom, K.-Y. Lee and I. K. Song, *J. Mol. Catal. A*, **248**, 21 (2006).
34. W. Kaleta and K. Nowińska, *Chem. Commun.*, 535 (2001).
35. N. K. Kala Raj, S. S. Deshpande, R. H. Ingle, T. Raja and P. Manikandan, *Catal. Lett.*, **98**, 217 (2004).
36. H. Kim, J. C. Jung, P. Kim, S. H. Yeom, K.-Y. Lee and I. K. Song, *J. Mol. Catal. A*, **259**, 150 (2006).
37. E. H. Hong, Y.-H. Jung and K.-H. Lee, *Korean J. Chem. Eng.*, **17**, 237 (2000).
38. H.-C. Jeong, I.-W. Shim, K. Y. Choi, J. K. Lee, J.-N. Park and C. W. Lee, *Korean J. Chem. Eng.*, **22**, 657 (2005).
39. P. Kim, J. B. Joo, J. Kim, W. Kim, I. K. Song and J. Yi, *Korean J. Chem. Eng.*, **23**, 1063 (2005).
40. D. Zhao, J. Feng, Q. Huo, N. Melosh, G. H. Frederickson, B. F. Chemlka and G. D. Stucky, *Science*, **279**, 548 (1998).
41. H. Kim, J. C. Jung, D. R. Park, S.-H. Baeck and I. K. Song, *Appl. Catal. A*, **320**, 159 (2007).
42. A. E. Shalagina, Z. R. Ismagilov, O. Y. Podyacheva, R. I. Kvon and V. A. Ushakov, *Carbon*, **45**, 1808 (2007).
43. J. R. Pels, F. Kapteijn, J. A. Moulijn, Q. Zhu and K. M. Thomas, *Carbon*, **33**, 1641 (1995).
44. P. H. Matter, L. Zhang, U. S. Ozkan, *J. Catal.*, **239**, 83 (2006).